Nanoscale Advances

ROYAL SOCIETY OF CHEMISTRY

COMMUNICATION

View Article Online
View Journal | View Issue

Cite this: *Nanoscale Adv.*, 2025, **7**, 4837

Received 14th April 2025
Accepted 26th June 2025

DOI: 10.1039/d5na00349k

rsc.li/nanoscale-advances

Rational impurity doping for enhanced hole mobility *in silicon* quantum dots for light-emitting diodes†

Hiroyuki Yamada, *[a] Tadaaki Nagao [a] and Naoto Shirahata *[ab]

We report on the impact of impurity doping on the performance enhancement of silicon quantum dot (SiQD) light-emitting diodes. The increase in hole mobility resulting from boron doping increases the external quantum efficiency of electroluminescence by a factor of 12 and the optical power density by a factor of 2.65.

Introduction

The main features that make the nanocrystal form of silicon (Si) interesting are that Si is naturally abundant and has no known biological toxicity,[1] along with being a typical indirect bandgap semiconductor. In spite of this indirect characteristic, bright fluorescence emissions based on quantum confinement effects, which occur when the nanocrystal size is equal to or smaller than the Bohr radius (~5 nm), can be observed.[2] Photoluminescence (PL) spectra are tuneable in the 530–1130 nm range by varying the diameter between 1.1 nm and 7.8 nm.[3] Such spectral tunability has attracted attention for application to optically active layers in the current-driven quantum dot light-emitting diodes (QLEDs). In 2010, Holmes and co-coworkers reported the first Si-QLED with an electroluminescence (EL) spectral peak at $\lambda = 868$ nm.[4] In the following year, several research groups reported red-visible light-emitting diodes.[5,6] The tuning range of EL spectra has also been expanded to a broad range between 590 nm and 1000 nm.[7,8] Moreover, white light emission was also achieved by taking advantage of the large Stokes shift between the absorption and emission spectra, which is an inherent characteristic of the unique energy structure of SiQDs.[9] The peak value of external quantum efficiency (EQE) of the red QLEDs based on SiQDs was ~4% in the early study,[6] rising to 6.2% in 2018.[10] Over the past three years, EQEs have exceeded 10%,[11] with a record value of 16.5% achieved in 2025.[12] While the EQE has come within reach of the industrial benchmark of 20%, a newly emerging concern is the low luminance. Specifically, such high EQEs have been observed at a very low applied bias voltage, close to the turn-on voltage. This is a common undesirable characteristic of Si-QLEDs: even a slight increase in current density leads to a rapid drop in EQE, unlike QLEDs based on other semiconductors, including CdSe, making it difficult to achieve high luminance while maintaining high efficiency. Watanabe and co-workers noted a lack of balanced energy diagram due to lower carrier mobility for holes compared to that for electrons in Si-QLEDs, resulting in suppressed luminance with increasing current density.[8] To address the challenge mentioned above, many attempts have been made to optimize the energy band alignment using various materials including molecules for the electron injection/transportation layer (EIL/ETL) and hole injection/transportation layer (HIL/HTL).[6,7,13] Another method is to use short ligands such as allylbenzene or octane as capping molecules on the QD surface.[10,14]

Heterovalent doping is achieved by intentionally incorporating an impurity ion that has a different valence from the host cation, providing extra electrons for n-type conductivity or extra holes for p-type conductivity. For Si crystals, boron and phosphorus are traditional dopants used to provide p- and n-type semiconductor Si. Recent results showing successful impurity doping in SiQDs have suggested the potential application of p-type and n-type conducting materials.[15] In 2024, we reported a solution-processing method for constructing a p–n homojunction architecture and demonstrated the fabrication of a p–n homojunction photodiode using p- and n-type SiQDs.[16] This result inspired us to use the doped QDs as an optically active layer in QLEDs to enhance carrier mobility. In this study, we attempt to enhance the carrier mobility for holes to achieve a balanced energy band diagram.

[a]*Research Center for Materials Nanoarchitectonics (MANA), National Institute for Materials Science (NIMS), 1-1 Namiki, Tsukuba 305-0047, Japan*

[b]*Graduate School of Chemical Science and Engineering, Hokkaido University, Kita 13, Nishi 8, Kita-ku, Sapporo 060-8628, Japan*

† Electronic supplementary information (ESI) available. See DOI: https://doi.org/10.1039/d5na00349k

Results and discussion

In accordance with our previous protocol,[16] boron-doped SiQDs capped with a monolayer of 10-undecanoic acid were prepared, as illustrated in Fig. 1(a) (see the Experimental section, ESI†). A typical XRD pattern of the hydrogen-capped p-type SiQDs is shown in Fig. 1(b). The diffraction peaks observed at $2\theta = 28°$, 47°, 56° were indexed to the (111), (220) and (311) planes of a diamond cubic Si lattice structure. The mean diameter calculated using the Williamson–Hall method was 1.9 ± 0.7 nm. It has been reported that the diameters of SiQDs smaller than 2 nm, as estimated from XRD peak broadening, are in good agreement with those measured by high-resolution transmission electron microscopy and small-angle X-ray scattering.[3] The hydrogen-terminated QD samples were characterized using various analytical techniques. First, there was no visible shift in the XRD peak positions when compared to the undoped sample (see Fig. S2, ESI†). Second, inductively coupled plasma optical emission spectrometry (ICP-OES) measurement indicated that only 0.21 mol% of boron was present in the sample synthesized with a nominal 5 mol% boron content, and 0.23 mol% when the nominal concentration was increased to 30 mol% during the synthesis. Third, the sample synthesized with nominal 5 mol% boric acid was characterized by X-ray photoelectron spectroscopy (XPS). The XPS B1s spectrum of the as-synthesized sample shows a dominant peak centered at 188 eV (see Fig. S3, ESI†), corresponding to the B–B bond. After 5 days of ambient exposure, the B^0 signal disappeared and was replaced entirely by B_2O_3 peaks, suggesting that the boron ions detected in the XPS B 1s spectrum resided on the SiQD surface and became oxidized over time in air. Consequently, the fraction of boron substitutionally incorporated into the SiQD lattice is assumed to be significantly low (well below 0.21 mol%), and any slight peak shift arising from minor lattice distortion or trace levels of substitutional boron may be obscured by the intrinsic broadness of the XRD peaks.

A Fourier transform infrared (FT-IR) spectrum of the p-type SiQDs terminated with undecanoic acid (UA) monolayers is presented in Fig. 1(c). The peaks in the range of 2960–2850 cm^{-1} and 1500–1350 cm^{-1} were attributed to the stretching and bending/scissoring modes of the C–H bond, respectively. The absorption in the 1735–1700 cm^{-1} range was attributed to the C═O stretching mode, indicating the termination of the Si surface with UA molecules. The broad peak observed at 1100–1000 cm^{-1} was attributed to the stretching mode of the O–Si–O bond, possibly due to surface oxidation during the thermal hydrosilylation reaction. The small peak observed in the range of 2140–2080 cm^{-1} indicated that Si–H_x bonds remained even after the hydrosilylation reaction.[8] As shown in Fig. 1(d), the PL spectrum displayed a peak centered at 765 nm with a full width at half maximum (FWHM) of 165.6 nm. The mean value of absolute PLQY was 16.7%. On the other hand, the undoped SiQDs exhibited a PL peak at 755 nm with a FWHM of 143.3 nm (Fig. S4, ESI†) and the mean value of absolute PLQY was 23.6%. Further experiments are needed to clarify the differences in spectral properties. This colloidal ink of p-type SiQDs was used as the optically active layer for Si-QLEDs.

The device architecture and its cross-sectional SEM image are presented in Fig. 2(a). Formation of the Ag electrode, MoO_3 HIL and TCTA HTL was performed using a vacuum evaporator,

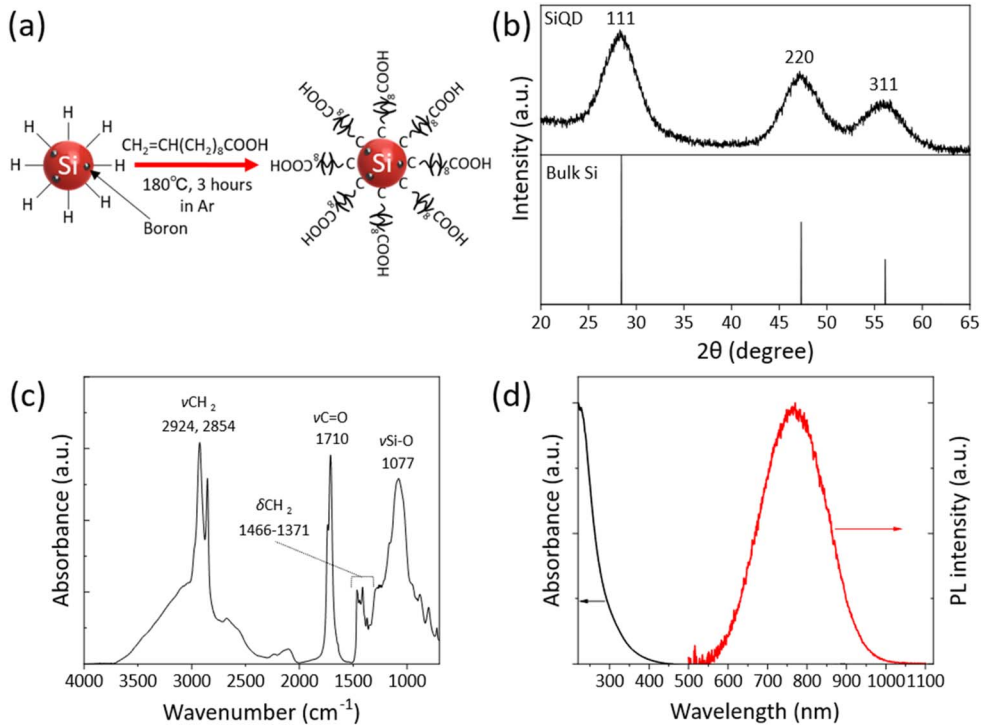

Fig. 1 (a) A schematic representation for the preparation process for B-doped SiQDs terminated with UA monolayers, (b) XRD pattern of hydrogen-capped SiQDs, (c) FTIR spectrum and (d) UV-VIS and PL spectra of the B-doped SiQDs terminated with UA monolayers.

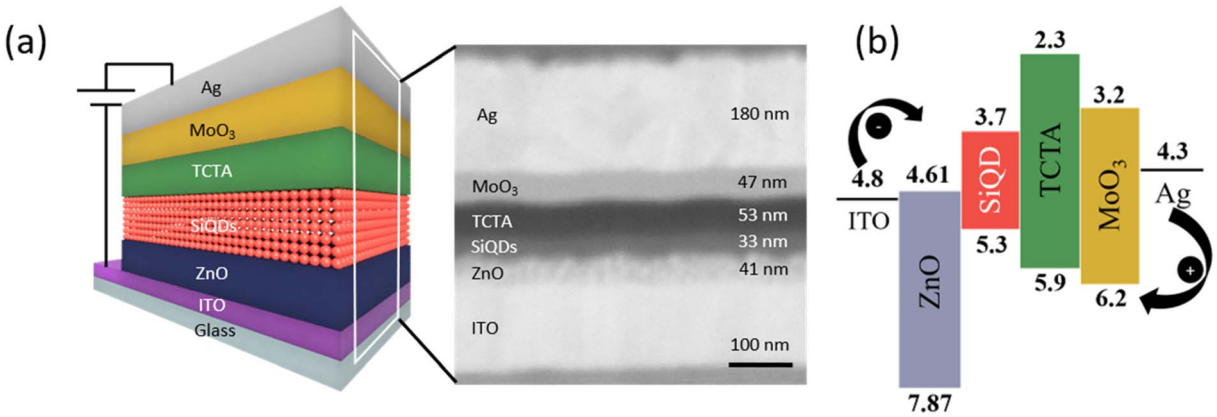

Fig. 2 (a) Schematic illustration of the Si-QLEDs with an inverted device structure and a cross-sectional SEM image of the device structure with a hybrid organic/inorganic multilayer stack, and (b) flat energy band diagram under unbiased conditions.

as depicted in Fig. S5, ESI.† We found that TCTA forms a flat, smooth and amorphous thin film structure without voids on the luminescent layer at an evaporation rate of 20 Å s^{-1}. The proposed flat energy band diagram under zero applied bias voltage is shown in Fig. 2(b). The valence band maximum (VBM) and conduction band minimum (CBM) of ZnO thin films were estimated from UPS and UV-VIS spectra (Fig. S6, ESI†). For the B-doped SiQDs, the VBM energy was 5.3 eV and the Fermi level position was close to the VBM, confirming p-type behaviour (see Fig. S7, ESI†). The values of TCTA and MoO_3 were taken from the literature.[17,18] Fig. 2(b) shows the favourable condition for effective electron injection from the electrode at a low applied bias voltage owing to the low energy barrier between ITO and ZnO. In addition, the deep VBM energy level of ZnO acted as a hole blocking barrier, confining holes within the active layer. Moreover, the high LUMO energy barrier of TCTA layers prevented the leakage of electrons to the adjacent anode, leading to enhanced radiative electron–hole recombination in the active layer for light emission.

Fig. 3 exhibits the device characteristics of the Si-QLED with an emission layer consisting of B-doped SiQDs while those of the Si-QLED with undoped SiQDs as a control are displayed. Panel (a) shows the current–voltage (*I–V*) characteristics while the optical power density characteristics as a function of voltage are shown in the panel (b). The values of turn-on voltage, defined as a voltage at which the optical power density is greater than 0.1 nW cm^{-2}, were 2.62 and 2.55 V for the Si-QLEDs with and without the boron dopant, respectively. The peak optical power density of the device with B-doped SiQDs was observed to be 169 μW cm^{-2} at 9.1 V. Then, the optical power density decreased as the applied voltage exceeded 9.2 V, even though the current density of the device continued to increase. On the other hand, the optical power density of the device with undoped SiQDs increased with increasing applied voltage, and almost saturated at 10 V. The estimated peak optical intensity was 63.7 μW cm^{-2}. In panel (c), the EQE values of each Si-QLED are plotted as a function of device current density. For each device, the EQE increased with increasing device current density, reaching peaks of 3.65% at 0.08 mA cm^{-2} and 0.3% at 3.1 mA cm^{-2}, and then began to decrease. This is probably due to Auger recombination that dominates the efficiency decrease at high current densities. We fabricated three Si-QLED devices of to evaluate the reproducibility of the EQE value. As shown in Fig. S8 (ESI),† the peak EQE reached 3.85% (see also Fig. S9, ESI†), while the other two devices exhibited 3.65%, indicating the reproducibility of boron doping in enhancing EQE. Panel (d) shows EL spectra of the device with B-doped SiQDs, measured at applied voltages ranging from 4 V to 9 V. The EL spectral peak at 4 V was observed at 765 nm, corresponding to the PL spectral peak, implying that EL originates from the SiQD layer. The EL spectra shifted relatively toward the shorter wavelengths with increasing applied voltage, and a peak was observed at 733 nm at 9 V. Observation of such a spectral shift is possibly due to the quantum confined Stark effect and/or band-filling effect that occur in the high device current density regime as commonly discussed in the literature.[19] In addition, the absence of parasitic EL from neighbouring layers even at 9 V indicates that the electrons injected from the electrode did not radiatively recombine in the ETL or HTL, but instead recombined with holes in the SiQDs to produce EL emission. As shown in the inset of panel (d), the luminance of the red EL was clearly uniform in a 2 × 2 mm region (see Fig. S1, ESI†), and no void emission was observed with the naked eye. This might be due to the hydrophilic property of the carboxylic-termination of QDs which improved the wettability with the underlying ZnO thin film.

In order to assess the electron and hole carrier mobilities of the B-doped SiQDs, an electron-only device (EOD) and a hole-only device (HOD) were fabricated in a manner similar to the Si-QLED (see Fig. S10, ESI†). The EOD consisted of ITO/ZnO/QDs/ZnO/Ag while the HOD consisted of ITO/PEDOT:PSS/TFB/QDs/TCTA/MoO_3/Ag. The carrier mobilities of both electrons and holes were estimated using the Space-Charge-Limited-Current (SCLC) model.[20] The calculation equation is as follows:

$$J = \frac{9}{8}\varepsilon_r\varepsilon_0\mu\frac{V^2}{d^3} \quad (1)$$

where J is the device current density, ε_r and ε_0 are the relative and vacuum dielectric constants, respectively. μ represents the field-independent carrier mobility, and d represents the

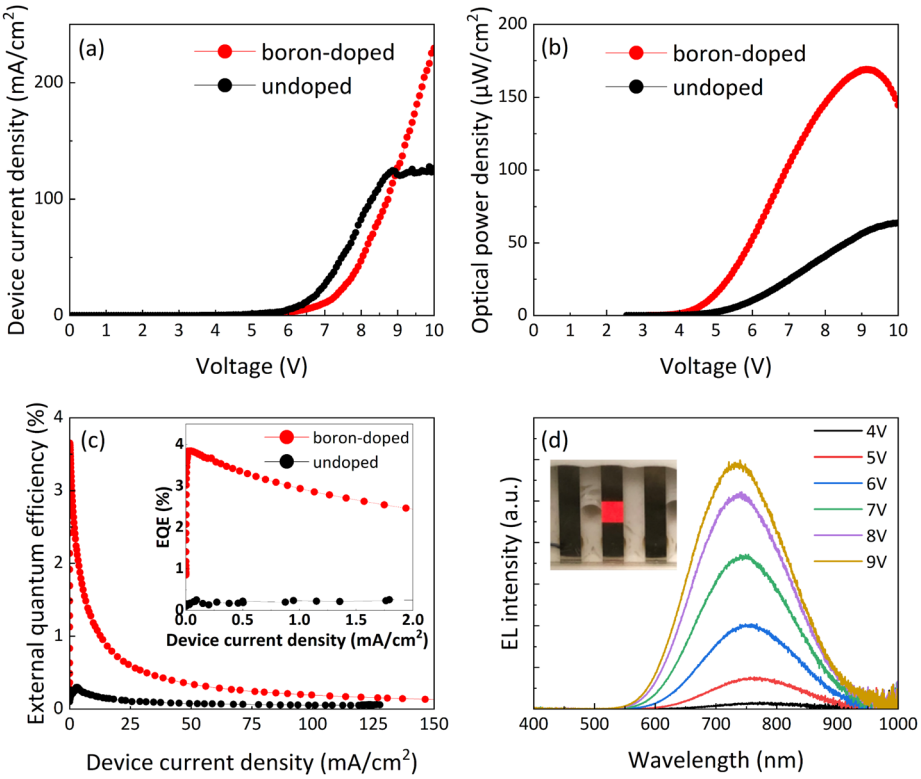

Fig. 3 Comparison of the device characteristics of B-doped and undoped Si-QLEDs: (a) *I*–*V* characteristics, (b) optical power density as a function of voltage, (c) plots of EQE as a function of device current density (the inset shows a zoomed-in view of the EQE dependence at current densities between 0 and 2 mA cm^{-2}) and (d) EL spectra of B-doped Si-QLEDs plotted at different applied voltages. The insets show a photograph of the device operating at 9 V.

thickness of the QD layer. In this study, ε_r and ε_0 are assumed to be 5.8 and 8.85 × 10^{-14} F cm^{-1} based on the literature.[20] The calculated charge injection ratios are presented in Table 1.

The B-doped SiQDs exhibit slightly lower electron mobility than undoped SiQDs, which is consistent with the typical behaviour observed in B-doped bulk Si. Conversely, the hole mobility of the B-doped SiQDs was found to be 3.38 times higher than that of the undoped SiQDs. This comparative analysis clearly demonstrates a significant improvement attributable to boron doping in SiQDs. Consequently, the carrier balance (μ_e/μ_h) in the B-doped SiQDs was improved by a factor of 6.49 compared to that of the undoped SiQDs. Although boron doping improves the carrier balance by a factor of 6.49, the resulting enhancement in EQE is approximately 12-fold. This discrepancy stems from the difference in current densities at which peak EQEs were recorded: 0.08 mA cm^{-2} for the B-doped device and 3.1 mA cm^{-2} for the undoped one. At such a high current density, the undoped device suffers from severe carrier imbalance and significant Auger recombination losses, which may result in an EQE that is up to 12 times lower than that of the B-doped device. Similarly, the limited increase in maximum optical power density (2.65-fold) in the B-doped device is likely attributable to Auger recombination dominating at high current densities induced by increased driving voltage.

Table 1 Electron (μ_e) and hole (μ_h) mobility results obtained within the SCLC model

SiQD	μ_e (cm^2 V^{-1} s^{-1})	μ_h (cm^2 V^{-1} s^{-1})	μ_e/μ_h
Boron-doped	$(3.91 \pm 0.45) \times 10^{-3}$	$(1.74 \pm 0.29) \times 10^{-5}$	224.713
Undoped	$(7.50 \pm 0.10) \times 10^{-3}$	$(5.14 \pm 0.61) \times 10^{-6}$	1459.14

Conclusions

We introduce a novel method for optimizing carrier balance in the active layer by incorporating B-doped SiQDs. Compared to Si-QLEDs using undoped SiQDs, those utilizing B-doped SiQDs exhibited significantly enhanced performance, with an EQE approximately 12 times higher and an optical power density about 2.65 times greater. Analysis of electron-only and hole-only devices revealed that boron doping decreases electron mobility in SiQDs while markedly increasing hole mobility by approximately 3.38-fold. Consequently, boron doping in SiQDs emerges as a promising strategy for adjusting electron and hole mobilities, thereby achieving balanced carrier transport within the active layer.

Data availability

The data that support the findings of this study are available from the corresponding author upon reasonable request.

Author contributions

H. Y. and N. S. designed the research, H. Y. performed the research, T. N. contributed to the analysis of the materials, H. Y., T. N. and N. S. discussed the results, and Y. H. and N. S. wrote the paper.

Conflicts of interest

There are no conflicts to declare.

Acknowledgements

The authors thank Takeo Ohsawa at NIMS for UPS measurements, Yuka Hara at NIMS for SEM observations, Takanobu Hiroto at NIMS for powder X-ray measurements and Yu Fujii at NIMS for ICP-OES measurements. This work was supported by the WPI program, ARIM of MEXT (JPMXP1225NM5200), JSPS KAKENHI grants (24K01462 and 24K21720) and the Hosokawa Powder Technology Foundation (HPTF24111). H. Y. thanks JSPS for the Research Fellowship and KAKENHI Grant-in-Aid (Grant No. 23KJ2166).

Notes and references

1 K. Yong, W. Law, R. Hu, L. Liu, M. T. Swihart and P. N. Prasad, *Chem. Soc. Rev.*, 2013, **42**, 1236; P. Reiss, M. Carrière, C. Lincheneau, L. Vaure, S. Tamang, B. Bruhn, B. JM Brenny, S. Dekker, I. Doğan, P. Schall and K. Dohnalová, *Light Sci. Appl.*, 2017, **6**, e17007; İ. N. G. Özbilgin, T. Yamazaki, J. Watanabe, H. T. Sun, N. Hanagata and N. Shirahata, *Langmuir*, 2022, **38**, 5188; G. Kim, G. Lee, M. Kang, M. Kim, Y. Jin, S. Beck, J. Cheon, J. Sung and J. Joo, *Faraday Discuss.*, 2020, **222**, 1236304.

2 L. Canham, *Faraday Discuss.*, 2020, **222**, 10; U. R. Kortshagen, R. M. Sankaran, R. N. Pereira, S. L. Girshick, J. J. Wu and E. S. Aydil, *Chem. Rev.*, 2016, **116**, 11061.

3 N. Shirahata, J. Nakamura, J. Inoue, B. Ghosh, K. Nemoto, Y. Nemoto, M. Takeguchi, Y. Masuda, M. Tanaka and G. A. Ozin, *Nano Lett.*, 2020, **20**, 1491.

4 K. Cheng, R. Anthony, U. R. Kortshagen and R. J. Holmes, *Nano Lett.*, 2010, **10**, 1154.

5 D. P. Puzzo, E. J. Henderson, M. G. Helander, Z. Wang, G. A. Ozin and Z. Lu, *Nano Lett.*, 2011, **11**, 1585; C.-C. Tu, L. Tang, J. Huang, A. Voutsas and L. Y. Lin, *Appl. Phys. Lett.*, 2011, **98**, 213102.

6 K. Cheng, R. Anthony, U. R. Kortshagen and R. J. Holmes, *Nano Lett.*, 2011, **11**, 1952.

7 F. Maier-Flaig, J. Rinck, M. Stephan, T. Bocksrocker, M. Bruns, C. Kübel, A. K. Powell, G. A. Ozin and U. Lemmer, *Nano Lett.*, 2013, **13**, 475; H. Yamada, N. Saitoh, B. Ghosh, Y. Masuda, N. Yoshizawa and N. Shirahata, *J. Phys. Chem. C*, 2020, **124**, 23333.

8 J. Watanabe, H. Yamada, H.-T. Sun, T. Moronaga, Y. Ishii and N. Shirahata, *ACS Appl. Nano Mater.*, 2021, **4**, 1165.

9 B. Ghosh, Y. Masuda, Y. Wakayama, Y. Imanaka, J. Inoue, K. Hashi, K. Deguchi, H. Yamada, Y. Sakka, S. Ohki, T. Shimizu and N. Shirahata, *Adv. Funct. Mater.*, 2014, **24**, 7151.

10 X. Liu, S. Zhao, W. Gu, Y. Zhang, X. Qiao, Z. Ni, X. Pi and D. Yang, *ACS Appl. Mater. Interfaces*, 2018, **10**, 5959.

11 H. Yamada, J. Watanabe, K. Nemoto, H. Sun and N. Shirahata, *Nanomater.*, 2022, **12**, 4314; Q. He, K. Wang, D. Li, D. Yang and X. Pi, *Adv. Opt. Mater.*, 2024, **12**, 2302422.

12 L. Wang, Y. Wada, H. Ueda, T. Hirota, K. Sumida, Y. Oba and K. Saitow, *Small Sci.*, 2025, 2400647.

13 L. Yao, T. Yu, L. Ba, H. Meng, X. Fang, Y. Wang, L. Li, X. Rong, S. Wang, X. Wang, G. Ran, X. Pi and G. Qin, *J. Mater. Chem. C*, 2016, **4**, 673–677; K. Saitow, *Bull. Chem. Soc. Jpn.*, 2024, **97**, uoad002.

14 M. L. Mastronardi, E. J. Henderson, D. P. Puzzo, Y. Chang, Z. Bin Wang, M. G. Helander, J. Jeong, N. P. Kherani, Z. Lu and G. A. Ozin, *Small*, 2012, **8**, 3647–3654.

15 N. J. Kramer, K. S. Schramke and U. R. Kortshagen, *Nano Lett.*, 2015, **15**, 5597; T. Velusamy, S. Mitra, M. Macias-Montero, V. Svrcek and D. Mariotti, *ACS Appl. Mater. Interfaces*, 2015, **7**, 28207; Y. Hori, S. Kano, H. Sugimoto, K. Imakita and M. Fujii, *Nano Lett.*, 2016, **16**, 2615; Z. Ni, X. Pi, S. Zhou, T. Nozaki, B. Grandidier and D. Yang, *Adv. Opt. Mater.*, 2016, **4**, 700; S. Chandra, Y. Masuda, N. Shirahata and F. Winnik, *Angew. Chem., Int. Ed.*, 2017, **56**, 6157; A. P. Y. Wong, W. Sun, C. Qian, A. A. Jelle, J. Jia, Z. Zheng, Y. Dong and G. A. Ozin, *Adv. Sustainable Syst.*, 2017, **1**, 1700118.

16 B. Ghosh, H. Yamada, K. Nemoto, W. Jevasuwan, N. Fukata, H. T. Sun and N. Shirahata, *Small Sci.*, 2024, **4**, 2400367.

17 H. Yamada, J. Watanabe, K. Nemoto, H. Sun and N. Shirahata, *Nanomaterials*, 2022, **12**, 4314.

18 H. Peng, W. Wang and S. Chen, *IEEE Electron Device Lett.*, 2015, **36**, 369–371.

19 D. Wang, J. Chen, J. Zhu, C. Lu and M. Lu, *J. Nanoparticle Res.*, 2013, **15**, 2063.

20 Q. Wan, Z. Li, C. Zhang, W. Zheng, L. Huang, M. Liu, Q. Zhang, B. Wang, W. Liu, L. Kong and L. Li, *J. Phys. Chem. C*, 2020, **124**, 28424.